energy&fuels

pubs.acs.org/EF

Article

Molecular Characterization of Remnant Polarizable Asphaltene Fractions Upon Bitumen Upgrading and Possible Implications in Petroleum Viscosity

Martha L. Chacón-Patiño,* Nicole Heshka, Anton Alvarez-Majmutov, Christopher L. Hendrickson, and Ryan P. Rodgers*

Cite This: *Energy Fuels* 2022, 36, 7542−7557

Read Online

ACCESS | Metrics & More | Article Recommendations

ABSTRACT: Thermal processing and hydrotreatment are used to decrease the viscosity of Alberta bitumen. However, changes in bulk properties, such as API gravity and viscosity, do not correlate to the gravimetric content of maltenes and asphaltenes. Thus, the work herein employs an extrography separation that yields asphaltene fractions enriched with distinct structural motifs and aggregation tendencies to investigate if changes in viscosity could be linked to the transformation or survival of specific asphaltene compounds and/or extrography fractions. Samples with limited change in viscosity upon thermal processing display minor changes in the gravimetric distribution of the extrography fractions, specifically polarizable species (Tol/THF/MeOH fraction). Ultrahigh-resolution mass spectrometry analysis demonstrates that such samples reveal neither a significant decrease in chemical polydispersity nor a change in the relative content of multicore/archipelago structural motifs post thermal treatment. Conversely, hydroprocessed samples with a pronounced viscosity reduction feature a remarkably lower chemical polydispersity and increased content of single-core (island) structural motifs. Polarizable asphaltene fractions from severely hydrotreated samples feature S-containing species with a low aromaticity, which on the basis of their molecular composition suggests that they are composed of the expected, alkyl substituted, geologically stable thiophenic cores (e.g., benzothiophene) as well as "unexpected" sulfides and sulfoxides. Collectively, the results suggest that the high viscosity of thermally upgraded samples could be correlated to the survival of asphaltene species with high heteroatom content (up to five heteroatoms per molecule) and persistent, high abundance of archipelago structural motifs. Thus, it is suspected that nanoaggregation of such fractions prevents their transformation into lighter products.

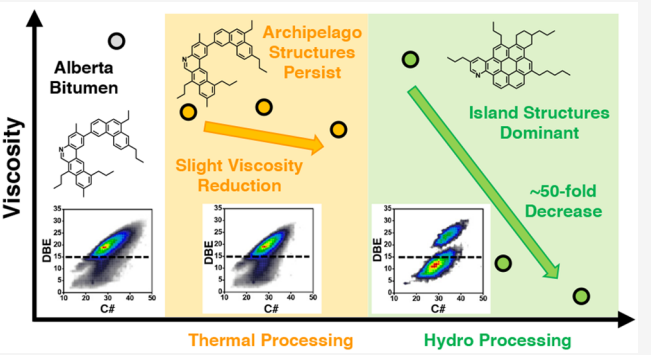

INTRODUCTION

Currently, continued petroleum industry efforts are focused on extra-heavy oils and oil sand bitumens due to the drastic depletion of light-to-medium oil reserves.[1] Furthermore, as the global energy sector aims to transition from fossil-based energy to renewable sources, asphaltene-enriched feedstocks are gaining interest due to their potential applications in material science, such as the production of low-cost carbon fibers.[2] However, the efficient use of extra-heavy fossil fuels has a fundamental constraint: their ultrahigh viscosity makes the recovery and transportation from production to processing facilities a challenging task in terms of required viscosity reduction and the effectiveness of simple dilution versus economic cost.[3]

Extra-heavy crude oils and bitumens feature high viscosity (>10 000 cPs) and high density (>1.0 g/mL) or low API gravity (<10.0), which is usually attributed to their high content of heteroatoms (O, N, S, V, and Ni) and increased asphaltene concentration compared to light and medium oils.[4,5] Therefore, petroleum companies usually perform *in situ* upgrading to improve the mobility of extra-heavy fossil fuels.[6] Generally, the goal of upgrading extra-heavy oils, *via* methods such as visbreaking and hydroconversion, is viscosity reduction, *via* cracking reactions to decrease molecular weight and/or disruption of intermolecular interactions that likely promote strong aggregation among specific petroleum fractions (e.g., asphaltenes).[7−13] Therefore, it is likely that viscosity reduction upon upgrading results from a decrease in

Received: May 12, 2022
Revised: June 21, 2022
Published: July 12, 2022

https://doi.org/10.1021/acs.energyfuels.2c01541
Energy Fuels 2022, 36, 7542−7557

the concentration of asphaltenes and resins, known for their higher heteroatom content and stronger aggregation tendencies. Viscosity improvement also arises from increasing the content of saturates and aromatics, with a concurrent decrease of the concentration of sulfur and other molecular features such as aromaticity.[14,15]

The improvement of methods for viscosity reduction *via in situ* upgrading requires comprehensive investigation of the molecular changes induced by cracking and addition reactions that occur during common processes such as thermal treatment and hydroprocessing. It is also critical to understand how these changes correlate with petroleum bulk properties (i.e., viscosity and API gravity). Indeed, there have been several attempts to establish correlations between viscosity and compositional features of crude oils.[16,17] Nevertheless, the prediction of the viscosity of complex mixtures, such as extra-heavy oils and their blends with lighter solvents, as a function of molecular composition, has been regarded as a highly complex task. For instance, Sjöblom et al.[17] reported correlations between viscosity values and the concentrations of the main components (saturates, aromatics, resins, and asphaltenes, SARA fractions) for 200 crude oil samples from various regions of Russia and the Norwegian continental shelf. The authors demonstrate a lack of consistent correlations between viscosity and the gravimetric distribution of SARA fractions for several groups of samples. For some crude oils, viscosity barely revealed even a general trend as a function of SARA composition. In other cases, for oils from different geological origins, there were strong correlations. For such oils, the viscosity increased as a function of increasing the content of asphaltenes, resins, and aromatics. Conversely, a higher concentration of saturates appeared to correlate with much lower viscosities. For some oils, asphaltenes, even at low concentrations (<2 wt %), appeared to be the major driver for high viscosity or low API.[17] Thus, asphaltenes are recognized for their possible central role in crude oil viscosity. It is believed that the nanoaggregates, the product of asphaltene self-association, are the main factor for the high viscosity of extra-heavy petroleum. However, Sjöblom et al.[17] also pointed out that the viscosity of asphaltene solutions (7−8 wt %) is only ∼60% higher than the viscosity of the respective pure solvent; therefore, the authors suggested that asphaltenes should be considered as moderate viscosity actors.

The work herein aims to understand the molecular composition of asphaltenes as a function of thermal conversion and hydroprocessing, and the role of specific asphaltene extrography fractions in viscosity changes observed upon upgrading. Alberta bitumen was upgraded *via* thermal cracking and hydroprocessing, under low, medium, and high severity conversion conditions for each. The feed and the upgraded oils were characterized by bulk measurements, including viscosity and density/API gravity measurements, and separated by solubility in *n*-heptane (maltenes vs asphaltenes content). This work focuses on a comprehensive characterization of asphaltenes to understand the effect of specific structural motifs and compound families on viscosity. For this purpose, *n*-heptane asphaltenes were isolated from the feed and the upgraded oils and subsequently fractionated by extrography. In this separation, asphaltenes are absorbed on silica gel and sequentially extracted in a Soxhlet apparatus with acetone, heptane/toluene, and toluene/tetrahydrofuran/methanol.[18] Thus, the separation yields three fractions with distinct composition and aggregation/precipitation behavior. Previous works demonstrate that acetone, a polar aprotic solvent with predominant dipolar interactions, assists the extraction of highly aromatic/alkyl-depleted asphaltenes with an increased content of single-core motifs, also known as island.[19] The intermediate solvent, heptane/toluene (1:1), enables the isolation of alkyl-aromatic species that experience no significant "polar" interactions with the silanol groups of the silica gel, with intermediate aromaticity. Finally, the protic mixture toluene/tetrahydrofuran/methanol (4:4:1) facilitates the extraction of species rich in polarizable functionalities, in some cases with much lower aromaticity than the preceding fractions, that are capable of hydrogen bonding to the SiO_2 silanol groups. This fraction has revealed increased amounts of multicore structural motifs, also known as archipelagos. Previous studies demonstrate that the acetone fractions extracted from asphaltenes obtained from diverse oils (Canadian bitumens, Wyoming, Venezuelan, Arabian Heavy, and Gulf of Mexico) feature weaker aggregation trends than Tol/THF/MeOH fractions, as revealed by size exclusion chromatography. Toluene solutions of the acetone extrography fractions were also shown to be the most stable when subsequently titrated with *n*-heptane.[20] The work presented herein investigates whether or not specific asphaltene fractions are dominant in upgraded samples with respect to changes/lack of changes in their viscosity relative to that of the feed. Ultrahigh-resolution mass spectrometry, specifically Fourier transform ion cyclotron resonance mass spectrometry (FT-ICR MS), is used as a molecular-level elemental analyzer as it provides the molecular formula for tens-of-thousands of ions and enables access to general trends between viscosity changes and molecular features such as aromaticity, heteroatom content, and atomic ratios such as H/C and S/C. The relative abundance of structural motifs, i.e., single-core vs multicore, is also accessed *via* gas-phase fragmentation, or tandem-MS *via* infrared multi-photon dissociation (IRMPD). The results suggest that the high viscosity of thermally upgraded samples could be due to the survival of species with high heteroatom content and increased levels of archipelago structural motifs. It is well-documented that such species concentrate in the Tol/THF/MeOH extrography fraction, which has revealed much stronger aggregation trends than the acetone and Hep/Tol fractions. Thus, it is likely that nanoaggregation prevents the transformation of these species into lighter products and ultimately impacts the ability of upgrading processes to decrease bitumen viscosity.

EXPERIMENTAL SECTION

Materials. High-performance liquid chromatography (HPLC)-grade *n*-heptane (Hep or nC_7), dichloromethane (DCM), toluene (Tol), acetone, and methanol (MeOH) were obtained from J.T. Baker (Phillipsburg, NJ) and used as received. Tetrahydrofuran (THF) with no solvent stabilizer was purchased from Alfa Aesar (Ward Hill, MA). Whatman filter paper grade 42 was used for asphaltene isolation from crude oils. High-purity glass microfiber thimbles were utilized for Soxhlet extractions (Whatman, GE Healthcare, Little Chalfont, U.K.). Chromatographic-grade silica gel (100−200 mesh, type 60 Å, Fisher Scientific) was used for extrography. Alberta bitumen (feed) and the liquid products from upgrading (i.e., thermal-processing TP and hydroprocessing HP) were supplied by CanmetENERGY Devon (Alberta, Canada).

Thermal-Processing (TP) and Hydroprocessing (HP). Thermal cracking of bitumen was conducted in a visbreaking pilot plant equipped with a 2 L/h continuously stirred tank reactor. These experiments were performed at cracking temperatures of 390−410 °C

https://doi.org/10.1021/acs.energyfuels.2c01541
Energy Fuels 2022, 36, 7542−7557

and residence times of ∼15−45 min in the reactor. Under these conditions, the conversion of material boiling above 525 °C (525 °C+ conversion) was maintained below 30% with the goal of coke management. The hydroprocessing of bitumen was carried out in a continuous pilot plant equipped with a tubular reactor packed with a commercial hydrotreating catalyst. The operating conditions were such that API gravity and viscosity were substantially improved, while minimizing fouling issues by sediment formation: temperature 380−400 °C, liquid hourly space velocity (LHSV) 0.3−1.0 h^{-1}, and pressure 6.9 MPa. The level of 525 °C+ conversion achieved through hydroprocessing was in the order of 25−54%. Feed and product analysis was done using standard methods: liquid density at 15.6 °C (ASTM D4052),[21] viscosity (ASTM D7042),[22] elemental analysis C/H/N (ASTM D5291),[23] and sulfur content (D4294).[24]

Asphaltene Precipitation from Feed and Upgraded Products, and Extrography Separation. nC_7 asphaltenes were isolated from the feed and the upgraded oils through a method reported elsewhere.[25] In short, the dropwise addition of *n*-heptane (400 mL) to the crude oil (10 mL) was carried out under sonication (Branson Ultrasonics, Danbury, CT, 22 kHz, and 130 W) and refluxed heating (∼90 °C). The mixture was allowed to stand for 12 h, and asphaltenes were subsequently collected by filtration, placed in a Soxhlet apparatus, and extracted with nC_7 for 72 h. Asphaltenes were recovered by dissolution in hot toluene (∼70 °C) and further cleaned *via* four cycles of asphaltene "crushing" and additional Soxhlet extraction with nC_7. This process aims to decrease the amount of coprecipitated/occluded maltenes in the asphaltene fraction.[25−27]

nC_7 asphaltenes from the feed and upgraded products were separated into fractions enriched in single-core or multicore motifs, by a shortened version of the extrography separation previously reported.[19] Briefly, 100 mg of asphaltenes was dissolved in DCM and mixed with 10 g of silica gel. The mixture was dried under a N_2 atmosphere. The solid mixture was placed in a Soxhlet apparatus and sequentially extracted with three solvents: acetone (100%), heptane/toluene (1:1, Hep/Tol), and toluene/THF/MeOH (4:4:1). Fractions were dried under N_2 and stored in amber vials for subsequent MS analyses.

Positive-Ion Atmospheric Pressure Photoionization Coupled to 9.4 T Fourier Transform Ion Cyclotron Resonance Mass Spectrometry [(+) APPI 9.4 T FT-ICR MS] and Infrared Multi-Photon Dissociation (IRMPD). Asphaltene samples were dissolved in toluene at a concentration of 100 μg/mL and directly infused into a Thermo-Fisher Ion Max APPI source (Thermo-Fisher Scientific, Inc., San Jose, CA). The APPI vaporizer was operated at 340 °C, N_2 sheath gas was used at 50 psi, and N_2 auxiliary gas was set at 32 mL/min. Gas-phase neutrals were photoionized by an ultraviolet Krypton lamp (∼10 eV). MS analyses were performed with a custom-built 9.4 T FT-ICR mass spectrometer equipped with a dynamically harmonized ICR cell.[28] Data collection and mass spectra calibration were assisted by custom PREDATOR software.[29] Selective isolation of high-DBE precursor ions for gas-phase fragmentation, or tandem-MS, was carried out by stored waveform inverse Fourier transform (SWIFT) as reported elsewhere.[30] The conditions for MS and IRMPD/MS analyses are reported in detail in the series *Advances in Asphaltene Petroleomics*.[26,30,31] Molecular formula assignment and data visualization were performed with PetroOrg N-18.3 Software.[32]

RESULTS AND DISCUSSION

Correlations Between Bulk Composition (maltene vs asphaltene content) and Viscosity Changes Upon Processing. Table 1 presents the API gravity and viscosity for the bitumen feed and the upgraded products from both thermal processing (TP) and hydroprocessing (HP), with each process performed under three conditions that yielded low/mild, medium, and high conversion. The results suggest that thermal processing is less effective in bitumen viscosity reduction than hydroprocessing, because in the former, the 525 °C+ conversion efficiency is restricted by coking and product stability. TP samples displayed only up to ∼1.5-fold decrease in viscosity, relative to the feed. Conversely, hydroprocessed samples, in particular HP-3, resulted in a viscosity reduction of ∼50-fold.

Table 1. API Gravity and Viscosity for the Bitumen Feed and the Upgrading Products upon Thermal Processing (TP) and Hydroprocessing (HP)

sample #	API gravity	density (g/mL) at 15.6 °C	viscosity (cSt) at 7 °C	525 °C+ conversion
feed	8.0	1.0146	∼16 100[a]	NA
TP-1	10.2	0.9987	11 811	16% (low severity)
TP-2	10.1	0.9993	12 260	20% (mid severity)
TP-3	10.1	0.9991	10 793	24% (high severity)
HP-1	15.6	0.9610	15 000	25% (low severity)
HP-2	18.9	0.9401	1200	39% conversion (mid severity)
HP-3	20.4	0.9307	300	54% conversion (high severity), on spec product

[a]Feed's viscosity was not determined at 7 °C. The lowest possible temperature for viscosity determination, for the studied feed, is 40 °C (∼16 100 cSt). Theoretical calculations by the standard method ASTM D341-03, on the basis of measured viscosity values at 40, 60, and 80 °C, predicted a viscosity of 2 068 686 cSt at 7 °C. Here, we report the viscosity of the studied Alberta bitumen at 40 °C for comparison purposes.

It is well-known that viscosity, in most cases, dramatically increases with asphaltene concentration. Moreover, several works suggest that viscosity/API gravity are directly correlated to the extent of asphaltene nanoaggregation.[33] Thus, to determine whether or not changes in viscosity, upon bitumen upgrading, are due to variations in asphaltene and maltene content, the feed and the upgrading products were separated into maltenes (toluene, nC_7 soluble) and asphaltenes (toluene soluble, nC_7 insoluble). Figure 1a presents the gravimetric yields for maltenes (yellow) and asphaltenes (black) and demonstrates that hydroprocessing produces higher amounts of maltenes than thermal treatment. Indeed, the TP-3 sample, with a viscosity of ∼10 793 cSt, reveals a ∼1.1-fold decrease in maltene concentration compared to the feed. On the contrary, the HP-2 and HP-3 samples, with much lower viscosities of 1220 and 300 cSt, present a ∼1.1-fold increase in maltene content. Albeit significant, such changes in the gravimetric content for maltenes and asphaltenes do not explain the dramatic viscosity variations for HP-2 (∼13-fold decrease) and HP-3 (∼54-fold decrease).

To access compositional trends that might explain such changes in viscosity upon processing, nC_7 asphaltenes were fractionated *via* extrography. Importantly, asphaltenes are ultracomplex mixtures whose direct characterization by MS is hindered by selective ionization.[34−39] Thus, a more comprehensive, molecular investigation is uniquely provided by coupling separation methods (e.g., extrography and chromatography) to FT-ICR MS. The extrography separation used in this work is based on the sample adsorption on SiO_2, and subsequent extraction with three solvents, i.e., acetone, Hep/Tol, and Tol/THF/MeOH. Acetone assists the isolation of highly aromatic/alkyl-depleted compounds with a predominant single-core (island) structure. The intermediate solvent, Hep/Tol, allows for the extraction of alkyl-aromatics. Finally, Tol/THF/MeOH targets the species that feature a higher polarizability and increased concentration of multicore (archipelago) structural motifs. It should be noted that there

https://doi.org/10.1021/acs.energyfuels.2c01541
Energy Fuels 2022, 36, 7542−7557

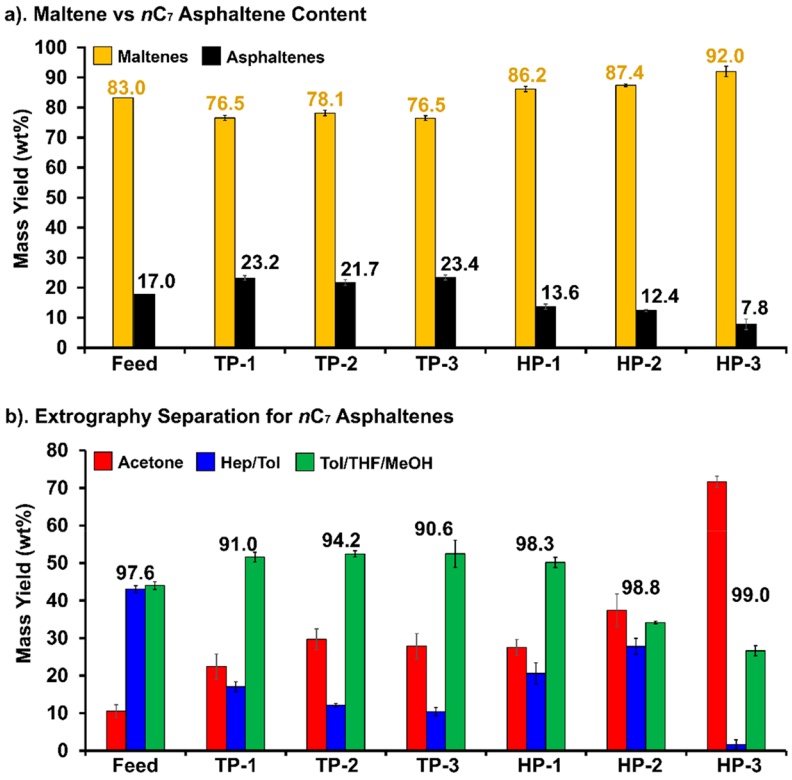

Figure 1. (a) Gravimetric yields for maltenes (C_7 soluble) and asphaltenes (C_7 insoluble) for the feed and the upgraded samples (thermally processed (TP) and hydroprocessed (HP)). (b) Gravimetric yields for the extrography separation of C_7 asphaltenes for the feed and the upgraded samples. Panel a includes the average values for yields for maltenes and asphaltenes. Panel b includes the average recovery (wt %) for the extrography separation, which ranges from 90.6 to 99.0 wt %.

is an asphaltene fraction that remains irreversibly adsorbed on the silica gel; the gravimetric yield of such species is sample dependent. In this study, the amount of irreversibly adsorbed material ranges from ~1 to 9 wt %. Figure 1b presents the gravimetric yields for the extrography fractions and exposes significant changes in samples that had a dramatic decrease (>10×) in viscosity. Specifically, Figure 1b points to a marked increase in concentration for the acetone fraction for the HP-3 sample (~6.8-fold), with a concurrent decrease for Hep/Tol (~26.5-fold) and Tol/THF/MeOH (~1.7-fold) as compared to the feed. In contrast, the upgraded sample with the lowest change in viscosity, HT-1, revealed a ~2.0-fold increase for the acetone fraction, a 2.5-fold decrease for Hep/Tol, and a slight increase in the Tol/THF/MeOH fraction.

Clearly, Figure 1b shows that, in asphaltenes from the hydroprocessed samples (HP-1−HP-3), the mass of the Tol/THF/MeOH fraction decreases consistently, even when the process is performed under high-severity conditions (HP-3). Note, the content of the Tol/THF/MeOH fraction (HP-1) initially increases ~1.2-fold compared to the feed. We hypothesize that such an increase could be due to the occurrence of secondary reactions between polar alkylaromatics,[40] which may yield asphaltene species with solubility parameters compatible with the Tol/THF/MeOH fraction. Although the upgrading process was performed on whole oils (mixture of maltenes and asphaltenes), the results suggest the interconversion between extrography-defined asphaltene subfractions: the decrease in Hep/Tol species (from feed to HP-1) is accompanied by an increase in both the acetone and Tol/THF/MeOH fractions.

HP-3 asphaltenes, from the products of the hydroprocessed bitumen under high severity conversion conditions, show a pronounced change in the gravimetric distribution of the extrographic fractions. Notably, the HP-3 sample reveals the lowest viscosity (~54-fold lower than that of the feed) and features the lowest levels of Hep/Tol and Tol/THF/MeOH fractions. This suggests a possible correlation between viscosity and the concentration of highly polarizable asphaltene species (i.e., Tol/THF/MeOH). It should be noted that the HP-1 sample, with a viscosity of ~15 000 cSt, has a Tol/THF/MeOH content of ~50 wt %. The HP-2 sample contains ~34 wt % of this extrography fraction and features a marked decrease in viscosity relative to HP-1 (~12-fold decrease). The change of the Tol/THF/MeOH content is less pronounced for the HP-3: it contains ~27 wt % and only reveals a ~ 4-fold drop in viscosity relative to HP-2. This suggests that polarizable Tol/THF/MeOH species, previously shown to exhibit stronger aggregation tendencies than acetone and Hep/Tol, could act as critical viscosity modifiers in crude oils. Furthermore, the results suggest that these species could survive hydroconversion under severe conditions. It is also likely that these molecules may be similar to those present in the starting material but not identical as a result of cracking/addition reactions. The following section focuses on the detailed molecular characterization of the asphaltene extrography fractions obtained from the feed and the upgraded samples.

Molecular Composition of Feed C_7 Asphaltenes Revealed by +APPI FT-ICR MS. Figure 2 presents the molecular composition of nC_7 asphaltenes isolated from the

https://doi.org/10.1021/acs.energyfuels.2c01541
Energy Fuels 2022, 36, 7542−7557

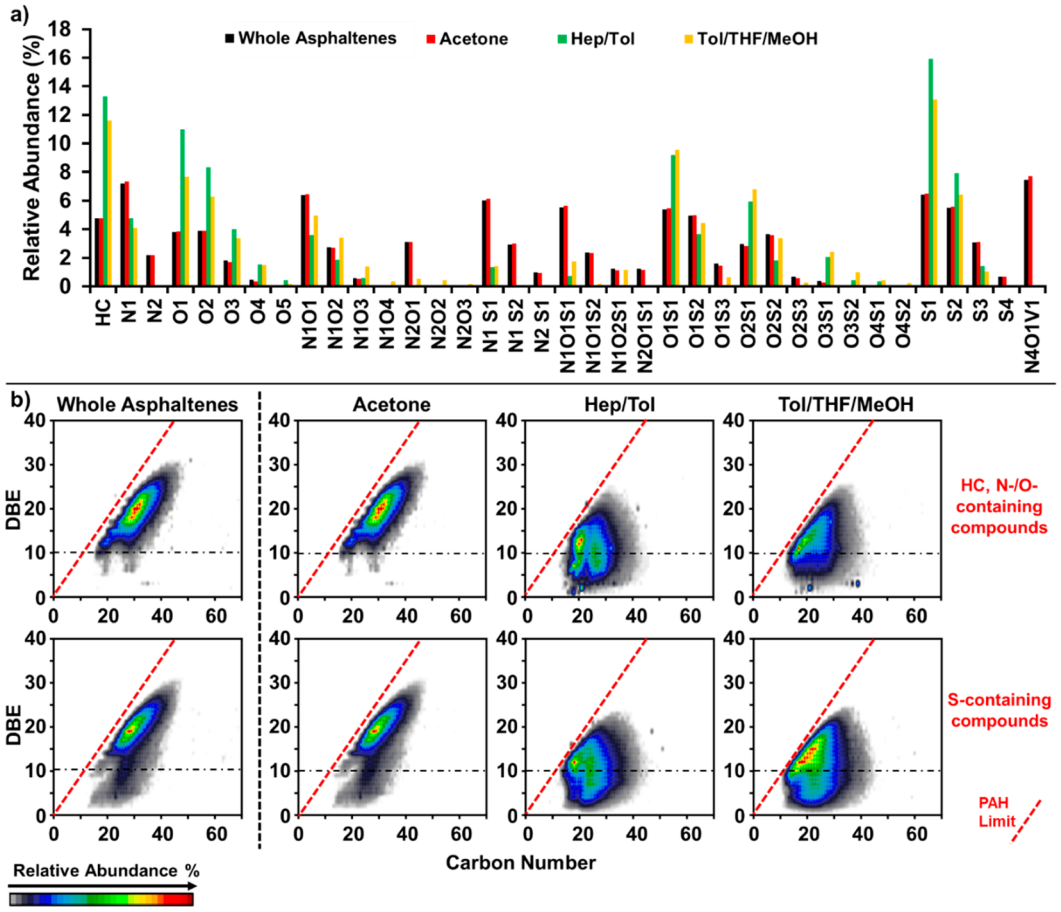

Figure 2. (a) Heteroatom class distribution for feed whole nC_7 asphaltenes and their extrography fractions. (b) Combined DBE vs carbon number plots for hydrocarbons (HC) and only N-/O-containing compounds (upper row) and all S-containing species (lower row) for whole asphaltenes and the fractions.

feed and the respective extrography fractions, analyzed by positive-ion APPI FT-ICR MS. The detected peaks in the mass spectra are assigned a unique molecular formula based on ultrahigh mass accuracy, uniquely provided by FT-ICR MS. Thus, the technique is used to directly track molecular changes in elemental compositions. Molecular formulas are sorted in heteroatom compound classes. For example, species with C, H, and two N atoms belong to the N_2 class. Figure 2a shows the compound class distribution for the whole/unfractionated feed asphaltenes, along with its acetone, Hep/Tol, and Tol/THF/MeOH fractions. As previously reported, asphaltene acetone fractions resemble the composition of whole/unfractionated samples.[31] It is important to point out that the acetone fraction displays the highest ionization efficiency in +APPI (also known as monomer−ion yield), and thus, it dominates the ionization of the whole sample. Thus, MS analysis of whole samples mostly reveals the species that comprise the acetone fraction. This behavior has been attributed, in part, to the decreased self-aggregation tendency of the acetone fraction, as compared to Hep/Tol and Tol/THF/MeOH fractions. Several works demonstrate that aggregation is linked to the efficiency of ion production in atmospheric pressure ionization (e.g., APPI, electrospray ionization).[41,42]

The results presented in Figure 2a highlight the wide diversity of compound classes for the whole asphaltenes and acetone fraction, with vanadyl porphyrins ($N_4O_1V_1$ class) as the dominant species given their efficient ionization in APPI.[43] The presence of compound classes with high heteroatom content, such as O_4, S_4, and O_2S_3, demonstrates the ultrahigh complexity and chemical polydispersity of the samples. Furthermore, whole asphaltenes and the acetone fraction reveal an increased abundances of species with N and S, such as N_1S_1, N_1S_2, and N_2S_1 classes (N_xS_y). Conversely, Hep/Tol and Tol/THF/MeOH fractions feature lower amounts of N-containing species, such as N_1, N_2, N_xS_y, and $N_xO_yS_z$, but higher abundances of polarizable O-containing molecules such as O_2, O_3, O_4, and compounds containing oxygen and sulfur atoms, such as O_2S_1, O_3S_1, and O_3S_2 classes. Importantly, vanadyl porphyrins are not detected in these extrography fractions. Previous studies suggest that vanadium complexes are indeed present in Hep/Tol and Tol/THF/MeOH fractions, but they remain undetected in APPI MS because they are predominately present in aggregates.[35,42,44]

Figure 2b presents combined plots of double bond equivalents (DBE) versus carbon number, commonly referred as "compositional range", for whole feed asphaltenes and the extrography fractions. DBE, or level of unsaturation, is the number of rings plus double bonds to carbon in a molecule and is calculated from the molecular formula obtained by FT-ICR MS. In the plots, the DBE values are presented in the *y*-axis, whereas the carbon number is included in the *x*-axis. The color scale represents the relative abundance of species within the given class. Compounds with the same DBE but varying numbers of carbon belong to the same homologous series and,

https://doi.org/10.1021/acs.energyfuels.2c01541
Energy Fuels 2022, 36, 7542−7557

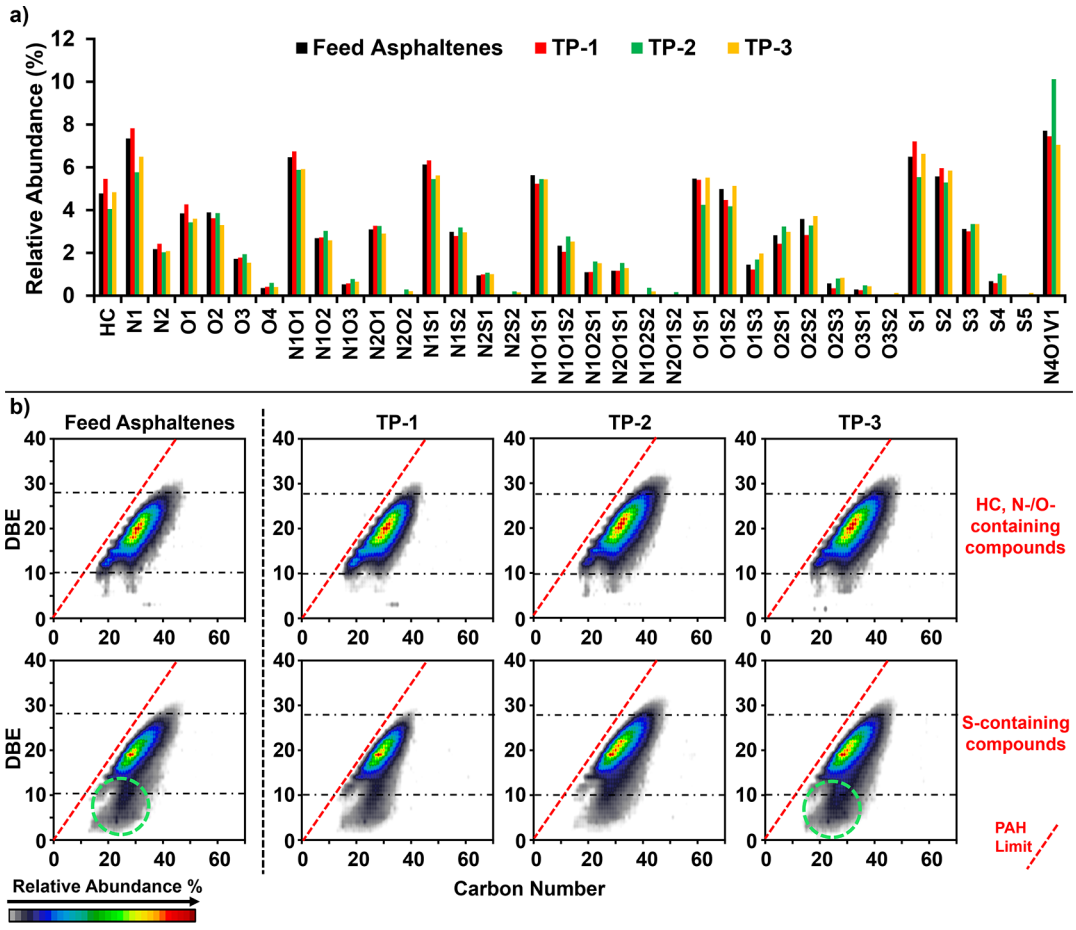

Figure 3. (a) Heteroatom class distribution and (b) combined DBE vs carbon number plots for hydrocarbons (HC) and only N-/O-containing compounds (upper row) and all S-containing species (lower row), for the acetone fractions isolated from the feed asphaltenes and the thermally processed samples.

thus, have the same number of rings and double bonds but differ in the number of saturated moieties (CH_2 units). For simplicity, Figure 2b presents combined DBE vs carbon number plots for hydrocarbons (HC class, molecules with no heteroatoms) and only O-/N-containing compounds (e.g., N_xO_y, N_x, and O_x, upper row). The lower row presents all the species that contain S atoms (e.g., S_x, N_xS_y, and $N_xO_yS_z$). As previously reported, the acetone fraction resembles the compositional range of whole asphaltenes: both samples, HC, N-/O-containing compounds feature high DBE values (>10) with abundant compounds close to the polycyclic aromatic hydrocarbon (PAH) limit, which is highlighted by the red-dotted line. The PAH limit is a compositional boundary for virgin fossil fuels. Species to the right, close to the PAH limit, are highly aromatic and alkyl-depleted.[45,46] An additional feature presented by the acetone fraction and whole asphaltenes is the "bimodal" compositional range for S-containing compounds: the dominant distribution (blue, green, yellow, red) is highly aromatic, with DBE values above ~13; it contains abundant compositions close to the PAH line. Conversely, the less abundant (black/gray) distribution reveals much lower DBEs, with carbon numbers far from the PAH limit. This suggests the likely presence of different S-containing chemical functionalities, such as thiophene, which tends to be highly aromatic, and sulfoxides/sulfides, known for their much lower aromaticity.[47,48]

Hep/Tol and Tol/THF/MeOH fractions reveal much lower DBE values, opposite to what is classically expected for asphaltenes.[49] Previous reports suggest that the low-DBE species detected in these fractions have a solubility behavior consistent with asphaltenes (toluene soluble/heptane insoluble) due to their increased heteroatom content and stronger aggregation tendency. These "atypical" species behave like asphaltenes (in terms of solubility) because of their high polarizability (molecular insolubility) and nanoaggregation (aggregate insolubility) and not because of aromaticity.[50,51]

Effect of Thermal Processing on Asphaltene Composition. Figure 3 presents the compound class distribution (panel a) and the compositional range (panel b) for the acetone fractions isolated from the nC_7 asphaltenes for the feed and the three thermally processed samples (TP). Information for whole TP C_7 asphaltenes is not included because the acetone fraction resembles the composition of unfractionated asphaltenes. The results indicate that thermal processing has no significant effect on the compound class distribution of the acetone-extracted species, as the TP samples reveal the same heteroatom classes, with similar relative abundances to those of the feed. The lower panel of Figure 3 suggests that thermal processing at high severity (TP-3) slightly broadens the compositional range for HC and N-/O-containing species in terms of homologous series length: TP-3 has 2−4 additional compositions per series than the feed. Furthermore, feed asphaltenes feature a global abundance weighted DBE of 19.5,

https://doi.org/10.1021/acs.energyfuels.2c01541
Energy Fuels 2022, 36, 7542−7557

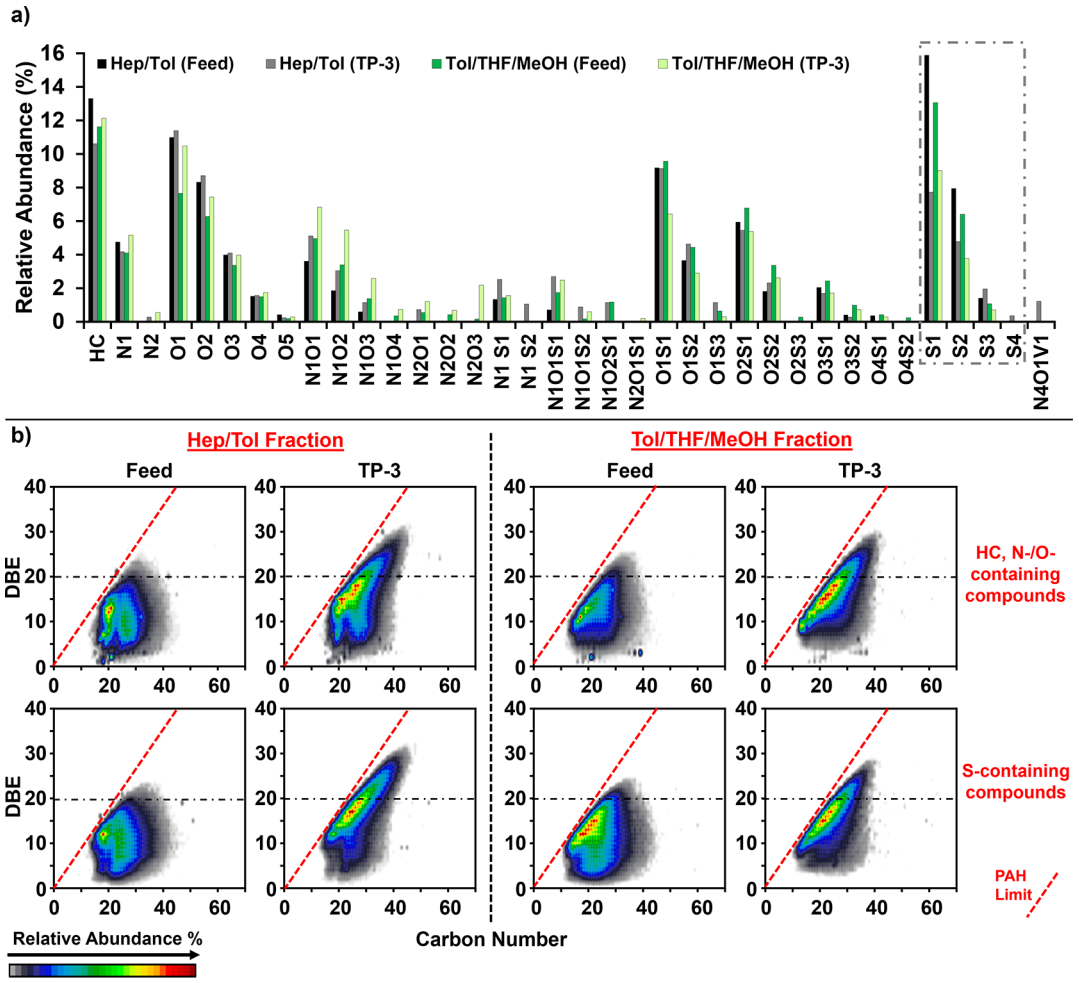

Figure 4. (a) Heteroatom class distribution and (b) combined DBE vs carbon number plots for hydrocarbons (HC) and only N-/O-containing compounds (upper row) and all S-containing species (lower row) for Hep/Tol and Tol/THF/MeOH extrography fractions isolated from the feed asphaltenes and the thermally processed TP-3 samples.

whereas the upgraded samples (TP-1, TP-2, and TP-3) reveal DBEs of 19.2, 20.5, and 19.9. The analysis of acetone fractions does not reveal significant changes in the molecular composition upon thermal processing. However, it is critical to point out that thermal process yields low molecular weight (LMW) species *via* cracking of bigger compounds originally present in the feed. A comparison of S-containing molecules in the feed and the TP-3 acetone fractions demonstrates, at some extent, the increase in the relative abundance (production) of species with lower DBE and carbon number upon processing (circled in green, Figure 3, lower panel). However, this change is not completely captured by Figure 3 since this works focuses on the molecular composition of asphaltenes, and many of the newly formed LMW species might be alkane soluble (maltenes). Below, we focus on Hep/Tol and Tol/THF/MeOH fractions to investigate the occurrence of reactions caused by upgrading processes that might explain the viscosity variations (Table 1) for the thermally processes samples.

Extrography Separation Reveals Molecular-Level Changes Induced by Thermal Processing. The TP-3 sample reveals the most significant changes in viscosity (~1.2-fold decrease relative to the feed). The analysis of the acetone fraction revealed no significant changes in terms of the heteroatom class distribution (chemical polydispersity) and the compositional range. Thus, to further investigate molecular-level changes induced by thermal processing, Figure 4 presents a comparison for the Hep/Tol and Tol/THF/MeOH fractions isolated from the nC_7 asphaltenes for the feed and TP-3 (the thermally processed sample with the largest change in viscosity). In Figure 4a, black/gray bars are used for the Hep/Tol fractions, whereas green-shade bars represent the Tol/THF/MeOH fractions. The results indicate that the thermal process causes no significant impact in bitumen chemical polydispersity, as the number of detected heteroatom classes is similar for the upgraded fractions and the feed. The major change is the decrease in the relative abundance of S_1 and S_2 classes for both extrography fractions. However, Figure 4b highlights extensive changes for the compositional range for the Hep/Tol and Tol/THF/MeOH extrography fractions. The feed features much lower DBE values (abundance weighted DBE up to ~12) and longer homologous series, which suggest the dominance of compounds with higher degrees of alkyl substitution and low aromaticity. After thermal processing, the fractions present abundant compositions close to the PAH limit, with much higher abundance-weighted DBE values (up to ~18) and shorter homologous series, which strongly suggests that thermal processing yields hydrogen deficient compounds with higher degrees of aromatic condensation. It should be noted that these changes in composition are

https://doi.org/10.1021/acs.energyfuels.2c01541
Energy Fuels 2022, 36, 7542−7557

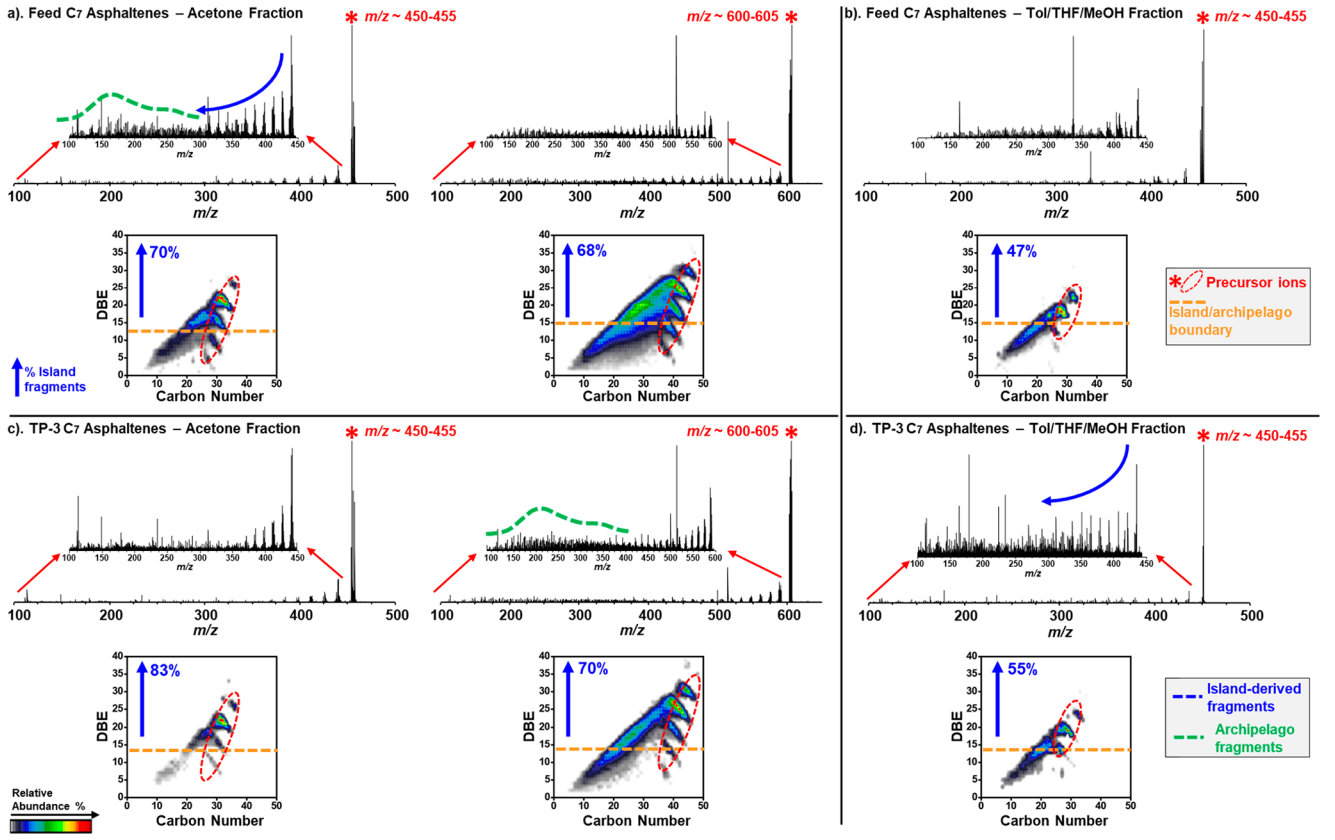

Figure 5. Fragmentation mass spectra and combined DBE vs carbon number plots for all compound classes with a relative abundance >1%, for precursor ions and fragments, for the acetone and Tol/THF/MeOH fractions for feed asphaltenes (panels a and b) and TP-3 asphaltenes (panels c and d).

uniquely accessed *via* separations, due to extensive selective ionization presented by complex petroleum samples.

Gas-Phase Fragmentation Reveals the Structural Motifs that Survive Upon Thermal Processing. The structural information for asphaltene ions was obtained *via* gas-phase fragmentation by infrared multi-photon dissociation (IRMPD). In this method, precursor ions from specific mass ranges are isolated using a quadrupole mass filter. Once the ions are transferred to the mass analyzer (i.e., ICR cell), a multi-notch SWIFT is applied to eject precursor ions with a low DBE. Thus, predominately high-DBE precursor ions remain trapped in the ICR cell for subsequent fragmentation by infrared irradiation. Figure 5 presents the fragmentation of predominantly high-DBE precursor ions, for the acetone and Tol/THF/MeOH fractions for the nC_7 asphaltenes for the feed (a, and b panels) and the thermally processed sample TP-3 (c and d panels). Figure 5 presents the fragmentation mass spectra with zoom insets that facilitate visualization for the mass range of the fragments. In the mass spectra, the precursor ions are highlighted with red asterisks. Two main fragmentation pathways are pointed out: the blue arrow indicates dealkylation; thus, the fragments decrease in carbon number but remain at the same DBE of the precursor ions, which is indicative for single-core/island structural motifs.[20] The second fragmentation pathway results in the low molecular weight distribution, highlighted in green. These fragments have a lower carbon number and lower DBE values than the precursor ions, which is indicative of multicore/archipelago structures. Figure 5 also includes DBE vs carbon number plots (all classes are combined) for fragments and precursor ions (circled in red) with a relative abundance of ≤1%. The orange dotted line included in the plots highlights the island/archipelago boundary, which is calculated from the mass spectra of the precursor ions. It is defined as the abundance weighted average DBE of the precursors minus the abundance weighted standard deviation. The percentage of fragments above that limit (highlighted in blue) provides the relative abundance of fragment ions originated from island structures. Fragments below the boundary are derived from archipelago precursors, and they feature much lower DBE values than those of the precursor ions. A concurrent loss of DBE and carbon number upon IRMPD is only possible when multicore structures are present in the selected mass range of precursor ions. For the acetone fractions, two mass ranges ($m/z \sim 450$ and 600) were evaluated. For Tol/THF/MeOH, only $m/z \sim 450$ is presented as the isolation of precursors with a higher molecular weight, which was challenging given their low relative abundance for this fraction. The fragmentation behavior of acetone fractions, for the feed and the TP-3 sample (panels a and c), indicates that the abundance of multicore/archipelago species slightly increases as a function of increasing m/z, which is consistent with previous reports.[34,52] After thermal processing, there is a slight increase in the relative abundance of single-core/island motifs (e.g., at m/z 450, from 70% to 83%).

The Tol/THF/MeOH fraction isolated from feed asphaltenes (panel b) reveals higher amounts of archipelago species at m/z 450 than the acetone fraction, which agrees with

https://doi.org/10.1021/acs.energyfuels.2c01541
Energy Fuels 2022, 36, 7542−7557

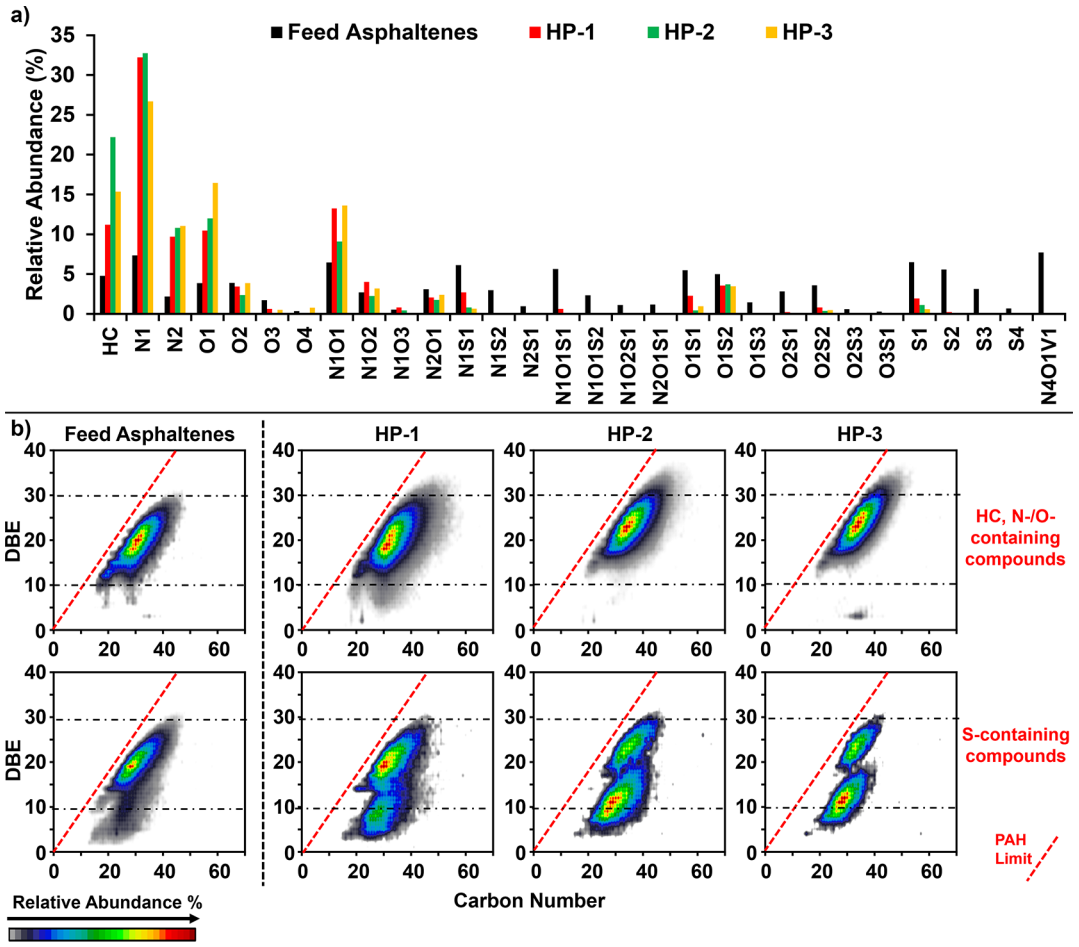

Figure 6. (a) Heteroatom class distribution and (b) combined DBE vs carbon number plots for hydrocarbons (HC) and only N-/O-containing compounds (upper row) and all S-containing species (lower row) for the acetone fractions isolated from the feed asphaltenes and the thermally processed TP-3 samples.

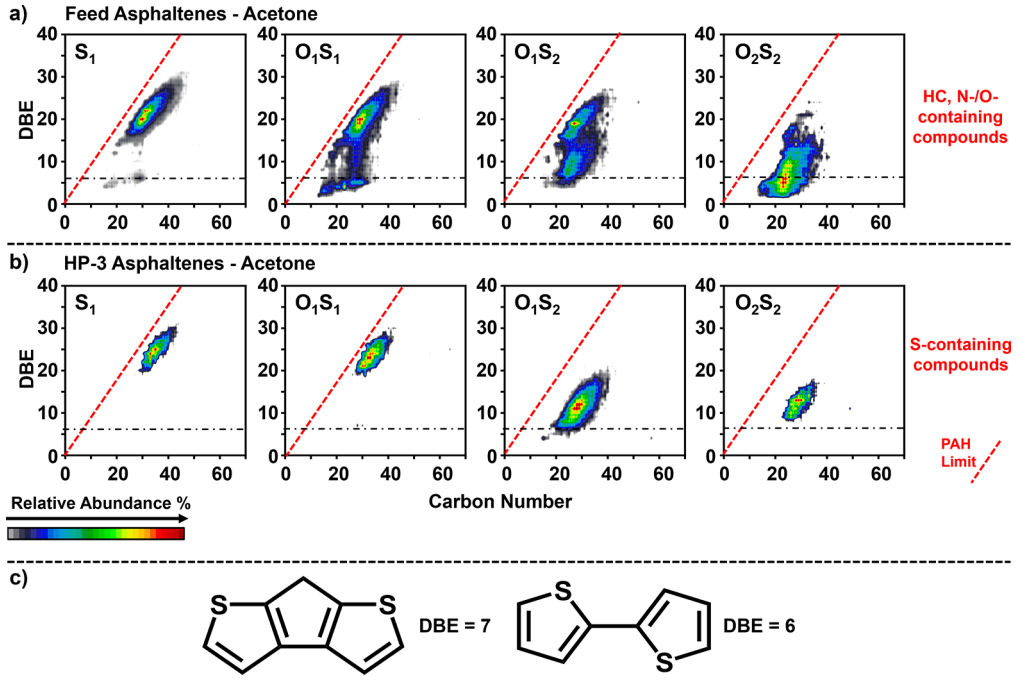

Figure 7. DBE vs carbon number plots for selected S-containing species for the acetone fraction from the (a) feed and (b) HP-3 sample. (c) Possible S-containing aromatic cores for DBE values of 6 and 7.

https://doi.org/10.1021/acs.energyfuels.2c01541
Energy Fuels 2022, 36, 7542−7557

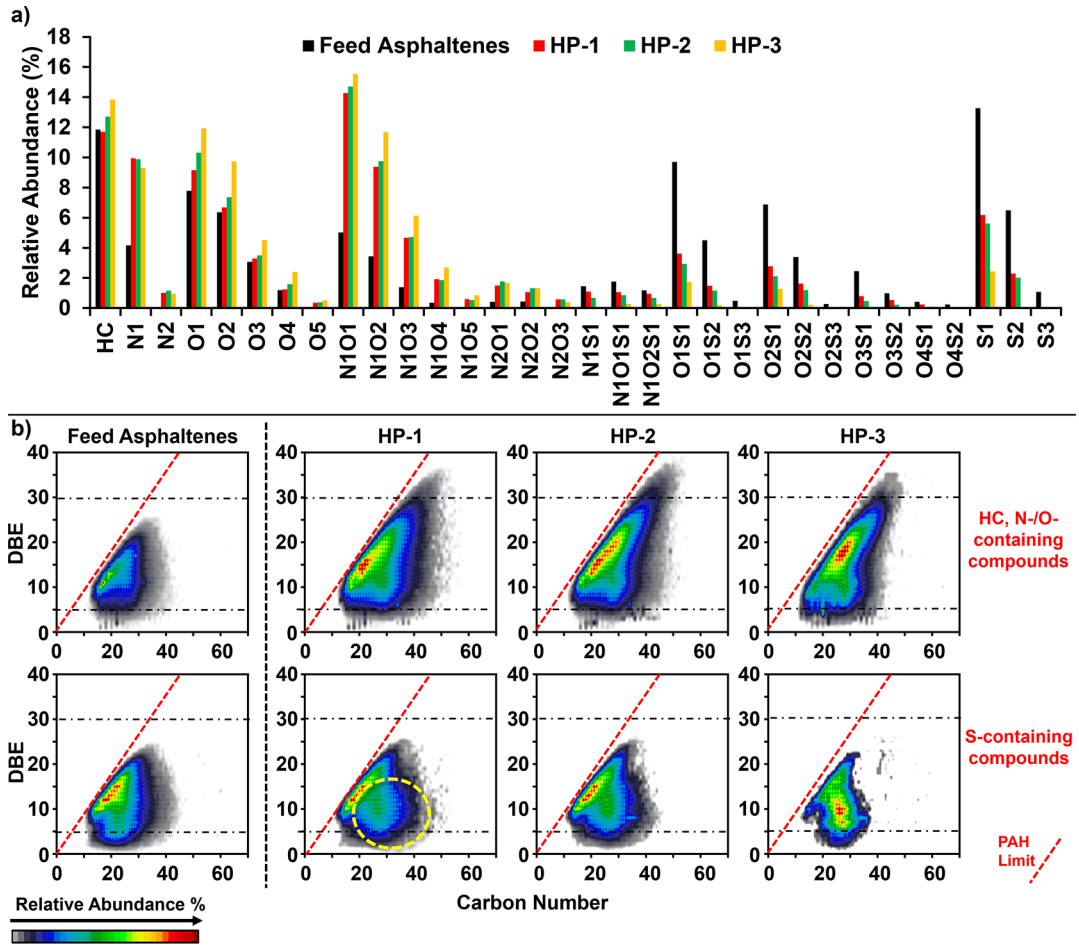

Figure 8. (a) Heteroatom class distribution and (b) combined DBE vs carbon number plots for hydrocarbons (HC) and only N-/O-containing compounds (upper row) and all S-containing species (lower row) for the Tol/THF/MeOH fractions isolated from the feed asphaltenes and the hydroprocessed (HP) samples.

previous studies.[20] After thermal treatment (sample TP-3, panel d), the amount of detected island-type structures slightly increased from 47% to 55%. Collectively, the results indicate that the thermal treatment used in this work fails to decrease asphaltene polydispersity in terms of heteroatom classes. However, the remaining asphaltene species feature a higher aromaticity and moderately increased content of island structural motifs.

Effect of Hydroprocessing on Asphaltene Composition. Figure 6 presents the compound class distribution for the acetone fractions isolated from the asphaltenes from the feed and the hydroprocessed samples (HP). The results demonstrate that hydroprocessing dramatically decreases the polydispersity of the products in terms of heteroatom classes, as the acetone fraction from feed asphaltenes contains 30 compound classes, whereas the HP sample series only has up to 17 classes. Species with a high number of heteroatoms, such as S_3, S_4, $N_4O_1V_1$, O_1S_3, and O_2S_3 classes, were not detected after hydroprocessing. Conversely, hydrocarbons with no heteroatoms (HC class), monoheteroatomic species (such N_1, O_1), and diheteroatomic classes (N_2, O_2, N_1O_1) became dominant in the hydroconverted acetone fractions. It should be noted that S-containing species dramatically decreased in abundance upon hydroprocessing, which suggests efficient hydrodesulfurization during the process.

Figure 6b shows that the compositional range for HC and N-/O-containing species shifts to higher DBE values, closer to the PAH limit as hydroprocessing severity increases, with the high conversion sample, HP-3, exhibiting the shortest homologous series. S-containing species reveal a distinctive behavior: upon hydroprocessing, the presence of two distributions (bimodal distribution highlighted earlier) is more pronounced. The HP-3 sample reveals a clear gap between both distributions, one at DBE values above 18, clustered along the PAH line, and the second one with predominant DBEs below 18 but displaced from the PAH limit. To further investigate this unique compositional feature, Figure 7 (a/b panels) highlights the compositional range of individual S-containing classes for the acetone fractions from the feed and the HP-3 sample. Interestingly, for both samples, classes with only one sulfur atom, S_1 and O_1S_1, reveal a compositional range enriched in high DBE species. Conversely, the O_1S_2 class reveals a bimodal compositional range for the feed; after hydroprocessing, only low DBE species (<20) are detected for this class. It is possible that, upon hydroconversion, high DBE O_1S_2 species are transformed into molecules belonging to classes with a lower number of heteroatoms, for instance, O_1S_1 and S_1, as a result of S and O atoms being contained in different aromatic cores (archipelago motifs) that are cracked during hydrotreatment.

https://doi.org/10.1021/acs.energyfuels.2c01541
Energy Fuels 2022, 36, 7542−7557

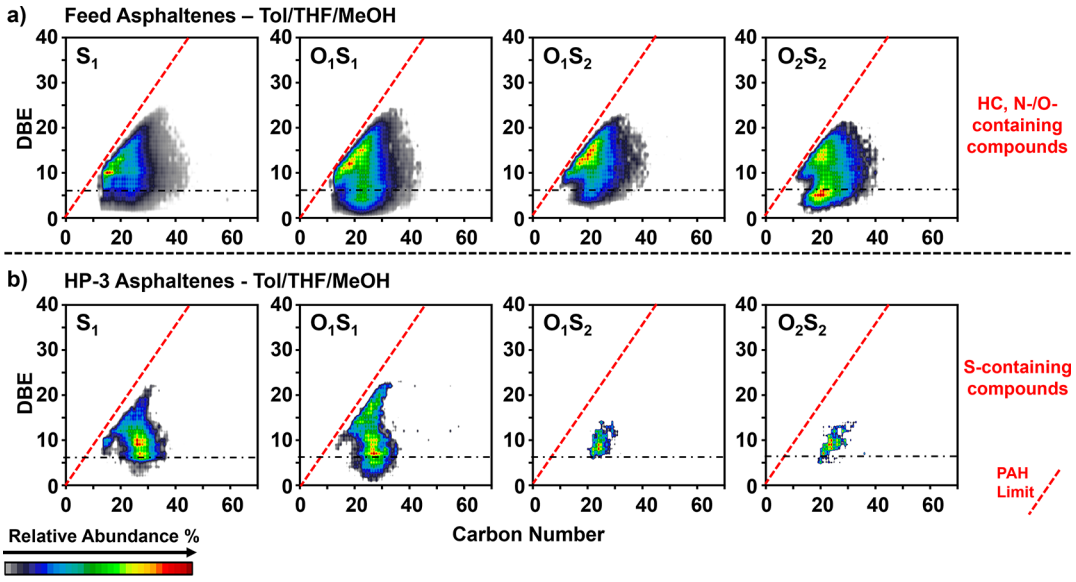

Figure 9. DBE vs carbon number plots for selected S-containing species for the Tol/THF/MeOH fractions from the (a) the feed and (b) HP-3 sample.

The survival of low DBE species upon severe hydroconversion is intriguing. However, a closer look to the DBE vs carbon number plots, before and after treatment, indicates that only compounds with a DBE higher ≥6 remain for O_1S_2 and O_2S_2 classes. One possibility is the existence of both sulfur atoms in cores such as cyclopenta-dithiophene or bithiophene, with DBEs of 6−7, as shown in Figure 7c. It is likely that both S moieties are protected by cycloalkyl and linear alkyl-side groups that prevent their cracking in hydroconversion. The lack of detection of compounds with DBE < 6−7 for the acetone HP-3 sample, suggests that these species are likely hydrodesulfurized and transformed into C_7-soluble compounds, which is consistent with previous reports.[53,54]

Compositional Trends for Hydroconverted Polarizable Asphaltene Fractions. Previous works demonstrate that the Tol/THF/MeOH fractions isolated from geologically diverse asphaltene samples (e.g., Athabasca bitumen, Maya, Venezuelan and Arabian heavy, and Wyoming deposit) reveal much stronger aggregation tendencies than acetone fractions and unfractionated asphaltenes.[20] This behavior has been attributed to the much higher polydispersity in terms of heteroatom content, due to the higher concentration of polyfunctional species (higher polarizability) and a higher diversity of structural motifs (higher abundance of archipelago motifs).[55] These compositional features likely translate into an aggregation mechanism involving several intermolecular forces, similar to the supramolecular assembly model proposed by Gray et al.[50,51] It has been suggested that such nanoaggregation can protect labile molecules, such as reactive biomarkers, from thermal degradation.[56,57] Indeed, it has been hypothesized that labile biomarkers were effectively protected inside asphaltene nanoaggregates, which contributed to their stability over geological time.[58,59]

Figure 8a presents the compound class distribution and compositional range for the Tol/THF/MeOH fractions isolated from the asphaltenes for the feed and the hydroprocessed (HP) samples. The results are in stark contrast to that of the acetone fractions (Figure 6) and indicate that all samples reveal a high complexity in terms of the number of heteroatom classes. Only the S-containing classes reveal the major changes due to processing, as they gradually decrease in relative abundance as a function of the process severity. In terms of the compositional range (Figure 8b), hydroconverted HC and N-/O-containing compounds reveal much higher DBE values than the feed. This could suggest the occurrence of dehydrogenation and/or addition reactions between alkyl-substituted aromatics of a lower molecular weight, which increases the DBE *via* hydrogen abstraction and/or production of multicore motifs. Moreover, the compositional range for the HP-3 reveals shorter homologous series than those of HP-1. In this regard, Gray et al.[40] reported that, upon upgrading, alkyl-substituted pyrene compounds undergo addition reactions through the alkyl-side groups, which originates bridged aromatic cores or archipelago products. Thus, the results indicate that alkyl-side groups constitute reactive moieties for thermal reactions, both cracking (dealkylation) and addition (production of multicore motifs).

On the contrary, hydroconverted S-containing compounds remain in the DBE range of the feed asphaltenes. However, it should be noted that abundant species with DBE from 2 to 5 also survive the upgrading process. Importantly, S-containing compounds in the Tol/THF/MeOH fraction reveal a bimodal compositional range: the dominant distribution for HP-1 and HP-2 samples is highly aromatic, clustered along the PAH line; the less abundant distribution (with lower DBE and higher carbon number) is highlighted in yellow. The presence of low DBE S-containing species before and after treatment, with a higher relative abundance than that of HC/N-/O-containing compounds, might suggest a selective occlusion of low-DBE S-containing molecules inside asphaltene networks. It is likely that the stronger nanoaggregation of Tol/THF/MeOH, highlighted in previous reports,[20,35,60] protects them from cracking into lighter fractions (e.g., gas, C_5−C_{20} alkanes).

To clarify compositional changes for S-containing compounds, Figure 9 highlights the DBE vs carbon number plots for selected compound classes. The results suggest that species with several S atoms (i.e., O_1S_2 and O_2S_2) are nearly eliminated, as their compositional range gets much narrower after hydroprocessing, and their relative abundance drops to near the limit of detection. Furthermore, the trends for S_1 and

https://doi.org/10.1021/acs.energyfuels.2c01541
Energy Fuels 2022, 36, 7542−7557

O_1S_1 compounds point to dealkylation as the main reaction pathway. It should be noted that the presence of low-DBE (<6) species for the O_1S_1 class after severe hydrotreatment suggests protection by nanoaggregation. It is likely that O_1S_1 compounds with DBEs of 2−5 are sulfoxides or O-containing sulfides. Indeed, when O atoms are not present (S_1 class), there is a detection of abundant homologous series with DBE values that correspond to well-known geologically stable structures such as alkyl-substituted benzo/dibenzothiophene. It is important to take into account that the upgrading process was carried out on whole bitumen and the reaction products are mixture of maltenes and asphaltenes; occlusion of heptane-soluble compounds inside asphaltene aggregates during sample preparation is possible and well-documented.[25,61,62]

Global Trends for Compositional Features Before and After Upgrading. Abundance weighted average molecular features, derived from FT-ICR MS data, such as DBE and atomic ratios (e.g., H/C, O/C) facilitate visualization of the compositional trends. Figure 10 presents the global abundance weighted S/C ratios, derived from all molecular formulas with their respective relative abundance, for each of the samples. The data is presented in gray and blue bars and includes the three extrography fractions (panels a−c) obtained from the nC_7 asphaltenes from the feed, the thermally processed samples, and the hydroconverted samples. Figure 10 also includes an abundance-weighted aromaticity factor, defined as the ratio of abundance-weighted DBE to abundance-weighted H/C. Thus, aromaticity is higher for species with a high DBE but a lower content of CH_2/saturated moieties (lower H/C).

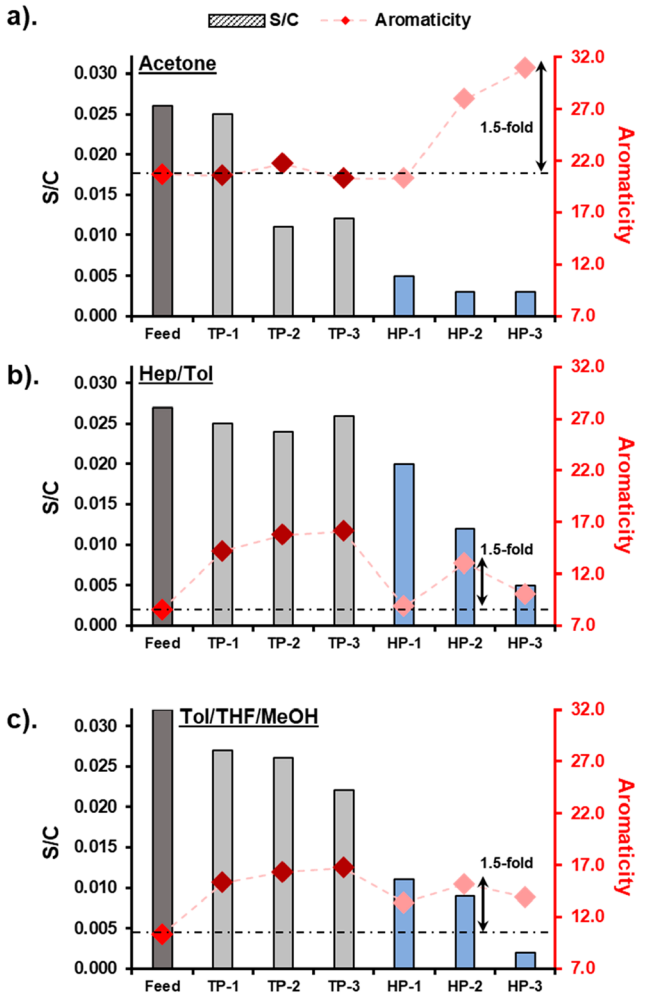

Figure 10. Global abundance weighted S/C ratios, for each of the samples (feed, thermally processed, and hydroconverted). The three extrography fractions are presented in panels a−c, obtained from the *n*C7 asphaltenes. The right *y*-axis is an abundance-weighted aromaticity factor.

Figure 10 shows that the acetone fractions exhibit the most pronounced changes upon processing. The hydroconverted acetone fractions feature the highest aromaticity; importantly, these samples presented the highest ionization efficiency during APPI MS analysis. Furthermore, the data shows that hydroprocessing yields a stronger decrease in S/C for all extrography fractions. Hydroconverted Hep/Tol and Tol/THF/MeOH fractions also reveal a stepwise decrease in S/C as a function of increasing process severity, and the most noticeable changes in aromaticity are presented by the HP-2 derived fractions, being ∼1.5-fold higher than the respective extrographic fraction from feed. It should be noted that thermal processing had a stronger effect on the aromaticity of the Hep/Tol and Tol/THF/MeOH fractions. During hydroprocessing, the aromaticity of these two fractions increases from HP-1 to HP-2, and then, it decreases for HP-3. This suggests that hydroprocessing under midseverity conditions likely causes addition reactions, which increases the fraction's aromaticity. However, high-severity conditions likely induce cracking of alkyl-bridges between aromatic cores of archipelagos, which, in the end, decreases aromaticity.

Effect of Hydroprocessing on Molecular Structure. Figure 11 presents the gas-phase fragmentation results for the hydroconverted acetone and Tol/THF/MeOH fractions. Again, the isolation of precursor ions at $m/z \sim 600$ for Tol/THF/MeOH was not possible due to a low relative abundance. The results demonstrate that hydroconversion is more efficient in the transformation of archipelago structural motifs, originally present in the feed, into island species. Specifically, IRMPD of precursor ions for the acetone fraction, with m/z around 450 and 600, revealed mostly island-derived fragments (100% and 98%). The results for Tol/THF/MeOH suggest that hydroconversion is more efficient in transforming highly "polar" multicore motifs into single core species, as the HP-3 Tol/THF/MeOH fraction revealed 79% of island-derived structural motifs, compared to only 55% detected for the thermally processed sample TP-3. Nevertheless, the results indicate the survival of some archipelago motifs (21%) that remain "intact" the in HP-3 Tol/THF/MeOH fraction.

CONCLUSIONS

Two upgrading methods, thermal processing and hydroconversion, were used to decrease the viscosity of Alberta bitumen. Changes in viscosity reveal no clear correlations to the gravimetric content of maltenes and asphaltenes. Thus, asphaltenes were fractionated by an extrography separation to investigate if changes in viscosity could be correlated to the transformation or survival of specific fractions and structural motifs.

The thermally processed bitumen, transformed under high-severity conditions, revealed a ∼1.5-fold decrease in viscosity. The thermal processed samples featured minor changes in the gravimetric distribution of the extrography fractions, in particular for polarizable species (Tol/THF/MeOH fraction).

https://doi.org/10.1021/acs.energyfuels.2c01541
Energy Fuels 2022, 36, 7542−7557

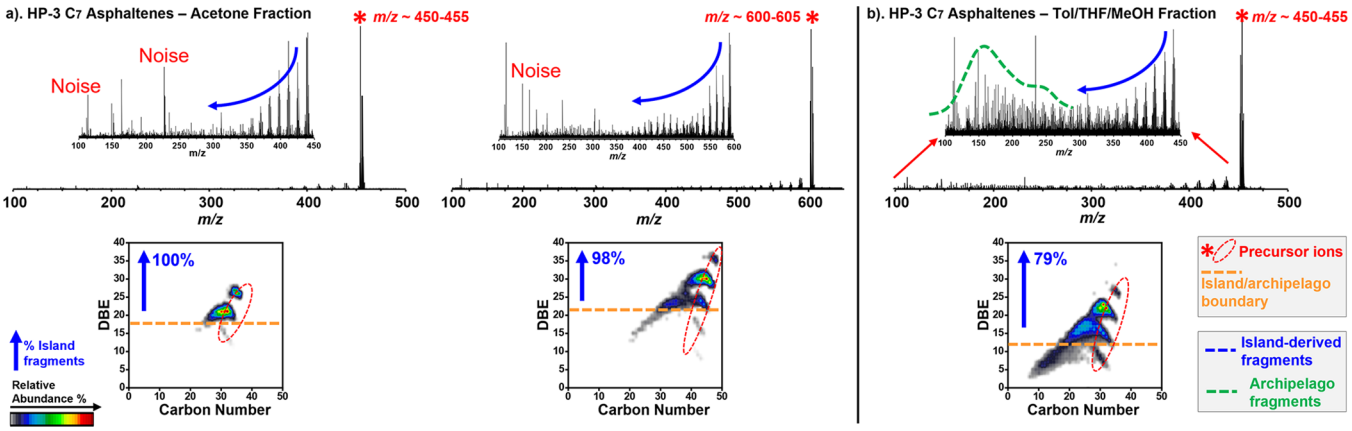

Figure 11. Gas-phase fragmentation spectra and compositional range for hydroconverted HP-3 asphaltene extrography fractions: (a) acetone and (b) Tol/THF/MeOH.

Molecular characterization of samples and extrography fractions, accessed *via* +APPI FT-ICR MS and IRMPD, demonstrates that the thermal process had no significant effect on the chemical polydispersity of the upgraded bitumen. The compound class distributions for all the extrography fractions after treatment revealed almost identical heteroatom classes with similar relative abundances as compared to the feed. However, thermal processing did produce changes in the compositional range of polarizable asphaltene species (Tol/THF/MeOH fraction). The process yielded abundant compositions closer to the PAH limit, with much higher abundance-weighted DBE values and shorter homologous series than those for the feed. These changes in composition were uniquely accessed *via* separations, due to extensive selective ionization in whole/unfractionated samples during direct MS analysis. Furthermore, gas-phase fragmentation demonstrated that thermal processing slightly increased the content of island structural motifs, e.g., from 70% to 83%, for acetone species.

Conversely, hydroprocessing caused significant changes in the gravimetric distribution of the asphaltene extrography fractions. In particular, there was a pronounced increase for acetone and decrease for Tol/THF/MeOH fractions. These changes may explain the dramatic drop in viscosity for the severely hydrotreated sample (>50-fold decrease compared to the feed). FT-ICR MS results demonstrate that hydroprocessing diminished the chemical polydispersity of acetone species; the fraction from the feed asphaltenes revealed 30 compound classes, whereas the hydroprocessed species only contained up to 17 classes. S-containing compounds revealed a unique feature upon hydroprocessing: the results highlighted the survival of low DBE species. A closer examination of the DBE vs carbon number plots, before and after treatment, indicates that molecules with DBEs higher ≥6 remain for classes with several S atoms, e.g., O_1S_2 and O_2S_2. We hypothesize the existence of both sulfur atoms in cores such as cyclopenta-dithiophene or bithiophene, likely protected by cycloalkyl/alkyl-side groups that prevent their cracking in hydroconversion.

The characterization of the hydroprocessed Hep/Tol and Tol/THF/MeOH extrography fractions indicates that the upgrading process was less effective in decreasing the chemical polydispersity of these species. Their compositional range suggests the occurrence of dehydrogenation and addition reactions between low-molecular-weight alkyl-substituted aromatics, which likely increases the DBE *via* hydrogen abstraction and production of multicore motifs. Furthermore, abundant O_1S_1 species with DBEs from 2 to 5 survived the process. It is likely that those O_1S_1 compounds are sulfoxides or O-containing sulfides, which remain intact under severe treatment conditions because the stronger nanoaggregation of Tol/THF/MeOH protects them from cracking and producing gas or C_5−C_{20} alkanes. Furthermore, gas-phase fragmentation demonstrates that hydroprocessing was more effective in transforming archipelago structural motifs into island species. For instance, the acetone fraction for the severely hydrotreated sample revealed ≥98% of island structural motifs.

Collectively, the results suggest that the high viscosity of the thermally processed bitumen could be correlated to the survival of species with high heteroatom content and increased abundance of archipelago structural motifs. Previous reports demonstrate that such species display much stronger aggregation trends than acetone and Hep/Tol and concentrate in the Tol/THF/MeOH extrography fraction, which was relatively constant regardless of the thermal processing severity and yielded only a slight decrease in viscosity. Thus, it is likely that nanoaggregation prevents the transformation of these species into lighter products.

Finally, the most intriguing results were noted for the hydroprocessed samples, where dramatic conversion/interconversion in and between extrography-defined asphaltene fractions was accompanied by large (up to ∼50-fold) changes in viscosity. The most severe hydroprocessing condition led to the near disappearance of the intermediate Hep/Tol extrography fraction, highest level of the acetone fraction, and continued reduction of the Tol/THF/MeOH species relative to less severe conditions. Although these dramatic changes in the extrography fractions are accompanied by equally dramatic changes in viscosity, linking changes in the molecular/supermolecular composition/structure with changes in viscosity is clearly still challenging. The current results suggest that, if the most aggregated material (Tol/THF/MeOH fraction) is a dominant contributor to increased viscosity, some subfraction of it remains susceptible to hydroconversion that alters the abundance of archipelago structures to produce unaggregated, acetone soluble species and near elimination of the intermediate Hep/Tol fraction.

https://doi.org/10.1021/acs.energyfuels.2c01541
Energy Fuels 2022, 36, 7542−7557

AUTHOR INFORMATION

Corresponding Authors

Martha L. Chacón-Patiño − *National High Magnetic Field Laboratory, Florida State University, Tallahassee, Florida 32310, United States*; Email: chacon@magnet.fsu.edu

Ryan P. Rodgers − *National High Magnetic Field Laboratory, Florida State University, Tallahassee, Florida 32310, United States; Department of Chemistry and Biochemistry, Florida State University, Tallahassee, Florida 32306, United States*; Email: rodgers@magnet.fsu.edu

Authors

Nicole Heshka − *Natural Resources Canada, CanmetENERGY, Devon, Alberta T9G 1A8, Canada*; orcid.org/0000-0002-8188-5888

Anton Alvarez-Majmutov − *Natural Resources Canada, CanmetENERGY, Devon, Alberta T9G 1A8, Canada*; orcid.org/0000-0002-6958-3959

Christopher L. Hendrickson − *National High Magnetic Field Laboratory, Florida State University, Tallahassee, Florida 32310, United States; Department of Chemistry and Biochemistry, Florida State University, Tallahassee, Florida 32306, United States*; orcid.org/0000-0002-4272-2939

Complete contact information is available at: https://pubs.acs.org/10.1021/acs.energyfuels.2c01541

Notes

The authors declare no competing financial interest.

ACKNOWLEDGMENTS

Work supported by NSF/DMR-1644779, Florida State University, and the State of Florida.

REFERENCES

(1) Gao, D.; Li, Z.; Liu, P.; Zhao, J.; Zhang, Y.; Li, C. A Coordinated Energy Security Model Taking Strategic Petroleum Reserve and Alternative Fuels into Consideration. *Energy* **2018**, *145*, 171−181.

(2) Saad, S.; Zeraati, A. S.; Roy, S.; Shahriar Rahman Saadi, M. A.; Radović, J. R.; Rajeev, A.; Miller, K. A.; Bhattacharyya, S.; Larter, S. R.; Natale, G.; Sundararaj, U.; Ajayan, P. M.; Rahman, M. M.; Kibria, M. G. Transformation of Petroleum Asphaltenes to Carbon Fibers. *Carbon N. Y.* **2022**, *190*, 92−103.

(3) Zhao, F.; Liu, Y.; Lu, N.; Xu, T.; Zhu, G.; Wang, K. A Review on Upgrading and Viscosity Reduction of Heavy Oil and Bitumen by Underground Catalytic Cracking. *Energy Reports* **2021**, *7*, 4249−4272.

(4) Li, X.; Chi, P.; Guo, X.; Sun, Q. Effects of Asphaltene Concentration and Asphaltene Agglomeration on Viscosity. *Fuel* **2019**, *255* (June), 115825.

(5) Shen, J.; Astrath, N. G. C.; Pedreira, P. R. B.; Guimarães, F. B.; Gieleciak, R.; Wen, Q.; Michaelian, K. H.; Fairbridge, C.; Malacarne, L. C.; Rohling, J. H.; Baesso, M. L. Correlations among Thermophysical Properties, Ignition Quality, Volatility, Chemical Composition, and Kinematic Viscosity of Petroleum Distillates. *Fuel* **2016**, *163*, 324−333.

(6) Ovalles, C.; Rogel, E.; Vien, J.; Morazan, H.; Carbognani-Ortega, L.; Lopez-Linares, F.; Rea, T.; Wei, T.; Miao, T.; Lee, E.; Moir, M. E. In-Situ Upgrading of Heavy Crude Oils via Solvent Deasphalting Using of Nickel Oxide Nanoparticles as Asphaltene Co-Precipitants. *Fuel* **2022**, *313*, 122707.

(7) Qu, X.; Li, Y.; Li, S.; Wang, J.; Xu, H.; Li, Z. Thermal Cracking, Aquathermolysis, and Their Upgrading Effects of Mackay River Oil Sand. *J. Pet. Sci. Eng.* **2021**, *201*, 108473.

(8) Ekramipooya, A.; Valadi, F. M.; Farisabadi, A.; Gholami, M. R. Effect of the Heteroatom Presence in Different Positions of the Model Asphaltene Structure on the Self-Aggregation: MD and DFT Study. *J. Mol. Liq.* **2021**, *334*, 116109.

(9) Nguele, R.; Okawa, H. Effect of Ultrasound Irradiation on Asphaltene Aggregation and Implications to Rheological Behavior of Bitumen. *Ultrason. Sonochem.* **2021**, *80*, 105811.

(10) Rahimi, P. Properties of Canadian Bitumen and Bitumen-Derived Crudes, and Their Impacts on Refinery Processing. In *Chemistry Solutions to Challenges in the Petroleum Industry*; ACS Symposium Series, Vol. *1320*, 2019; Chapter 8; pp 223−240.

(11) Rahimi, P. M.; Gentzis, T.; Chung, K.; Nowlan, V.; DelBianco, A. Correlation of Chemical Composition of Extra Heavy Oils with Incipient Coke Formation Using Hot-Stage Microscopy. *ACS Div. Fuel Chem. Prepr.* **1997**, *42* (1), 146−148.

(12) Rahimi, P. M.; Teclemariam, A.; Taylor, E.; DeBruijn, T.; Wiehe, I. A. Thermal Processing Limits of Athabasca Bitumen during Visbreaking Using Solubility Parameters. *Heavy Hydrocarbon Resources Chapter 13*; ACS Symposium Series, Vol. *895*, 2005; pp 183−196.

(13) Rahimi, P.; Gentzis, T.; Dawson, W. H.; Fairbridge, C.; Khulbe, C.; Chung, K.; Nowlan, V.; DelBianco, A. Investigation of Coking Propensity of Narrow Cut Fractions from Athabasca Bitumen Using Hot-Stage Microscopy. *Energy Fuels* **1998**, *12*, 1020−1030.

(14) Alarbah, A.; Shirif, E.; Jia, N.; Bumraiwha, H. A New Approach Utilizing Liquid Catalyst for Improving Heavy Oil Recovery. *J. Energy Resour. Technol. Trans. ASME* **2021**, *143* (7), 073006.

(15) Rueda-Velásquez, R. I.; Gray, M. R. A Viscosity-Conversion Model for Thermal Cracking of Heavy Oils. *Fuel* **2017**, *197*, 82−90.

(16) Djimasbe, R.; Varfolomeev, M. A.; Al-Muntaser, A. A.; Yuan, C.; Suwaid, M. A.; Feoktistov, D. A.; Rakhmatullin, I. Z.; Milovankin, A. A.; Murzakhanov, F.; Morozov, V.; Gafurov, M.; Farhadian, A.; Davletshin, R. R. Deep Insights into Heavy Oil Upgrading Using Supercritical Water by a Comprehensive Analysis of GC, GC-MS, NMR, and SEM-EDX with the Aid of EPR as a Complementary Technical Analysis. *ACS Omega* **2021**, *6* (1), 135−147.

(17) Malkin, A. Y.; Rodionova, G.; Simon, S.; Ilyin, S. O.; Arinina, M. P.; Kulichikhin, V. G.; Sjöblom, J. Some Compositional Viscosity Correlations for Crude Oils from Russia and Norway. *Energy Fuels* **2016**, *30* (11), 9322−9328.

(18) Chacón-Patiño, M. L.; Moulian, R.; Barrère-Mangote, C.; Putman, J. C.; Weisbrod, C. R.; Blakney, G. T.; Bouyssiere, B.; Rodgers, R. P.; Giusti, P. Compositional Trends for Total Vanadium Content and Vanadyl Porphyrins in Gel Permeation Chromatography Fractions Reveal Correlations between Asphaltene Aggregation and Ion Production Efficiency in Atmospheric Pressure Photoionization. *Energy Fuels* **2020**, *34* (12), 16158−16172.

(19) Chacón-Patiño, M. L.; Rowland, S. M.; Rodgers, R. P. Advances in Asphaltene Petroleomics. Part 2: Selective Separation Method That Reveals Fractions Enriched in Island and Archipelago Structural Motifs by Mass Spectrometry. *Energy Fuels* **2018**, *32* (1), 314−328.

(20) Chacón-Patiño, M. L.; Gray, M. R.; Rüger, C.; Smith, D. F.; Glattke, T. J.; Niles, S. F.; Neumann, A.; Weisbrod, C. R.; Yen, A.; McKenna, A. M.; Giusti, P.; Bouyssiere, B.; Barrère-Mangote, C.; Yarranton, H.; Hendrickson, C. L.; Marshall, A. G.; Rodgers, R. P. Lessons Learned from a Decade-Long Assessment of Asphaltenes by Ultrahigh-Resolution Mass Spectrometry and Implications for Complex Mixture Analysis. *Energy Fuels* **2021**, *35* (20), 16335−16376.

(21) *Standard Test Method for Density, Relative Density, and API Gravity of Liquids by Digital Density Meter, D4052−18a*; ASTM International: West Conshohocken, PA, 2018.

(22) *Standard Test Method for Dynamic Viscosity and Density of Liquids by Stabinger Viscometer (and the Calculation of Kinematic Viscosity), D7042−21a*; ASTM International: West Conshohocken, PA, 2021.

(23) *Standard Test Methods for Instrumental Determination of Carbon, Hydrogen, and Nitrogen in Petroleum Products and Lubricants, D5291−21*; ASTM International: West Conshohocken, PA, 2021.

(24) *Standard Test Method for Sulfur in Petroleum and Petroleum Products by Energy Dispersive X-Ray Fluorescence Spectrometry, D4294–21*; ASTM International: West Conshohocken, PA, 2021.
(25) Chacón-Patiño, M. L.; Vesga-Martínez, S. J.; Blanco-Tirado, C.; Orrego-Ruiz, J. A.; Combariza, M. Y.; et al. Exploring Occluded Compounds and Their Interactions with Asphaltene Networks Using High-Resolution Mass Spectrometry. *Energy Fuels* **2016**, *30* (6), 4550−4561.
(26) Chacón-Patiño, M. L.; Rowland, S. M.; Rodgers, R. P. Advances in Asphaltene Petroleomics. Part 1: Asphaltenes Are Composed of Abundant Island and Archipelago Structural Motifs. *Energy Fuels* **2017**, *31* (12), 13509−13518.
(27) Giraldo-Dávila, D.; Chacón-Patiño, M. L.; McKenna, A. M.; Blanco-Tirado, C.; Combariza, M. Y. Correlations Between Molecular Composition and the Adsorption, Aggregation and Emulsifying Behavior of Petrophase 2017 Asphaltenes and Their TLC Fractions. *Energy Fuels* **2018**, *32* (3), 2769−2780.
(28) Kaiser, N. K.; Quinn, J. P.; Blakney, G. T.; Hendrickson, C. L.; Marshall, A. G. A Novel 9.4 T FTICR Mass Spectrometer with Improved Sensitivity, Mass Resolution, and Mass Range. *J. Am. Soc. Mass Spectrom.* **2011**, *22* (8), 1343−1351.
(29) Blakney, G. T.; Hendrickson, C. L.; Marshall, A. G. Predator Data Station: A Fast Data Acquisition System for Advanced FT-ICR MS Experiments. *Int. J. Mass Spectrom.* **2011**, *306* (2−3), 246−252.
(30) Rodgers, R. P.; Marshall, A. G.; Niles, S. F.; Chacón-Patinõ, M. L.; Smith, D. F. Comprehensive Compositional and Structural Comparison of Coal and Petroleum Asphaltenes Based on Extrography Fractionation Coupled with Fourier Transform Ion Cyclotron Resonance MS and MS/MS Analysis. *Energy Fuels* **2020**, *34* (2), 1492−1505.
(31) Chacón-Patiño, M. L.; Rowland, S. M.; Rodgers, R. P. Advances in Asphaltene Petroleomics. Part 3. Dominance of Island or Archipelago Structural Motif Is Sample Dependent. *Energy Fuels* **2018**, *32* (9), 9106−9120.
(32) Corilo, Y. E. *PetroOrg. Software*; Florida State University, 2013.
(33) Padula, L.; Balestrin, L. B. D. S.; Rocha, N. D. O.; De Carvalho, C. H. M.; Westfahl, H.; Cardoso, M. B.; Sabadini, E.; Loh, W. Role of Asphaltenes and Additives on the Viscosity and Microscopic Structure of Heavy Crude Oils. *Energy Fuels* **2016**, *30* (5), 3644−3651.
(34) Nyadong, L.; Lai, J.; Thompsen, C.; LaFrancois, C. J.; Cai, X.; Song, C.; Wang, J.; Wang, W. High-Field Orbitrap Mass Spectrometry and Tandem Mass Spectrometry for Molecular Characterization of Asphaltenes. *Energy Fuels* **2018**, *32* (1), 294−305.
(35) Chacón-Patiño, M. L.; Moulian, R.; Barrère-Mangote, C.; Putman, J. C.; Weisbrod, C. R.; Blakney, G. T.; Bouyssiere, B.; Rodgers, R. P.; Giusti, P. Compositional Trends for Total Vanadium Content and Vanadyl Porphyrins in Gel Permeation Chromatography Fractions Reveal Correlations between Asphaltene Aggregation and Ion Production Efficiency in Atmospheric Pressure Photoionization. *Energy Fuels* **2020**, *34* (12), 16158−16172.
(36) Chacón-Patiño, M. L.; Blanco-Tirado, C.; Orrego-Ruiz, J. A.; Gómez-Escudero, A.; Combariza, M. Y. High Resolution Mass Spectrometric View of Asphaltene-SiO_2 Interactions. *Energy Fuels* **2015**, *29* (3), 1323−1331.
(37) Thomas, M. J.; Jones, H. E.; Palacio Lozano, D. C.; Gavard, R.; Carney, S.; Barrow, M. P. Comprehensive Analysis of Multiple Asphaltene Fractions Combining Statistical Analyses and Novel Visualization Tools. *Fuel* **2021**, *291*, 120132.
(38) Podgorski, D. C.; Corilo, Y. E.; Nyadong, L.; Lobodin, V. V.; Bythell, B. J.; Robbins, W. K.; McKenna, A. M.; Marshall, A. G.; Rodgers, R. P. Heavy Petroleum Composition. 5. Compositional and Structural Continuum of Petroleum Revealed. *Energy Fuels* **2013**, *27* (3), 1268−1276.
(39) da Silva, L. C.; Davila, J. V.; Fleming, F. P.; Combariza, M. Y.; Vaz, B. G. Laser Desorption Ionization and Collision Induced Dissociastion as Powerful Tools for FT-ICR Mass Spectrometric Characterization of Asphaltene Fractions Enriched in Island and Archipelago Motifs. *Fuel* **2022**, *323*, 124418.
(40) Alshareef, A. H.; Scherer, A.; Tan, X.; Azyat, K.; Stryker, J. M.; Tykwinski, R. R.; Gray, M. R. Formation of Archipelago Structures during Thermal Cracking Implicates a Chemical Mechanism for the Formation of Petroleum Asphaltenes. *Energy Fuels* **2011**, *25* (5), 2130−2136.
(41) Rodgers, R. P.; Mapolelo, M. M.; Robbins, W. K.; Chac, M. L.; Putman, J. C.; Niles, S. F.; Rowland, S. M.; Marshall, A. G. Combating Selective Ionization in the High Resolution Mass Spectral Characterization of Complex Mixtures. *Faraday Discuss.* **2019**, *218*, 29−51.
(42) Putman, J. C.; Moulian, R.; Barrère-Mangote, C.; Rodgers, R. P.; Bouyssiere, B.; Giusti, P.; Marshall, A. G. Probing Aggregation Tendencies in Asphaltenes by Gel Permeation Chromatography. Part 1: Online Inductively Coupled Plasma Mass Spectrometry and Offline Fourier Transform Ion Cyclotron Resonance Mass Spectrometry. *Energy Fuels* **2020**, *34*, 8308−8315.
(43) Ramírez-Pradilla, J. S.; Blanco-Tirado, C.; Hubert-Roux, M.; Giusti, P.; Afonso, C.; Combariza, M. Y. Comprehensive Petroporphyrin Identification in Crude Oils Using Highly Selective Electron Transfer Reactions in MALDI-FTICR-MS. *Energy Fuels* **2019**, *33* (5), 3899−3907.
(44) Zheng, F.; Zhang, Y.; Zhang, Y.; Han, Y.; Zhang, L.; Bouyssiere, B.; Shi, Q. Aggregation of Petroporphyrins and Fragmentation of Porphyrin Ions: Characterized by TIMS-TOF MS and FT-ICR MS. *Fuel* **2021**, *289*, 119889.
(45) Cho, Y.; Kim, Y. H.; Kim, S. Planar Limit-Assisted Structural Interpretation of Saturates/Aromatics/Resins/Asphaltenes Fractionated Crude Oil Compounds Observed by Fourier Transform Ion Cyclotron Resonance Mass Spectrometry. *Anal. Chem.* **2011**, *83* (15), 6068−6073.
(46) Lobodin, V. V.; Marshall, A. G.; Hsu, C. S. Compositional Space Boundaries for Organic Compounds. *Anal. Chem.* **2012**, *84*, 3410−3416.
(47) Lobodin, V. V.; Robbins, W. K.; Lu, J.; Rodgers, R. P. Separation and Characterization of Reactive and Non-Reactive Sulfur in Petroleum and Its Fractions. *Energy Fuels* **2015**, *29* (10), 6177−6186.
(48) Qiao, P.; Harbottle, D.; Tchoukov, P.; Masliyah, J.; Sjöblom, J.; Liu, Q.; Xu, Z. Fractionation of Asphaltenes in Understanding Their Role in Petroleum Emulsion Stability and Fouling. *Energy Fuels* **2017**, *31* (4), 3330−3337.
(49) Mullins, O. C.; Sabbah, H.; Eyssautier, J.; Pomerantz, A. E.; Barré, L.; Andrews, A. B.; Ruiz-Morales, Y.; Mostowfi, F.; McFarlane, R.; Goual, L.; Lepkowicz, R.; Cooper, T.; Orbulescu, J.; Leblanc, R. M.; Edwards, J.; Zare, R. N. Advances in Asphaltene Science and the Yen-Mullins Model. *Energy Fuels* **2012**, *26*, 3986−4003.
(50) Gray, M.; Tykwinski, R.; Stryker, J.; Tan, X. Supramolecular Assembly Model for Aggregation of Petroleum Asphaltenes. *Energy Fuels* **2011**, *25*, 3125−3134.
(51) Gray, M. R.; Yarranton, H. W.; Chacón-Patiño, M. L.; Rodgers, R. P.; Bouyssiere, B.; Giusti, P. Distributed Properties of Asphaltene Nanoaggregates in Crude Oils: A Review. *Energy Fuels* **2021**, *35* (22), 18078−18103.
(52) Dong, X.; Zhang, Y.; Milton, J.; Yerabolu, R.; Easterling, L.; Kenttämaa, H. I. Investigation of the Relative Abundances of Single-Core and Multicore Compounds in Asphaltenes by Using High-Resolution in-Source Collision-Activated Dissociation and Medium-Energy Collision-Activated Dissociation Mass Spectrometry with Statistical Consid. *Fuel* **2019**, *246*, 126−132.
(53) Rueda-Velásquez, R. I.; Freund, H.; Qian, K.; Olmstead, W. N.; Gray, M. R. Characterization of Asphaltene Building Blocks by Cracking under Favorable Hydrogenation Conditions. *Energy Fuels* **2013**, *27*, 1817−1829.
(54) Gray, M. R.; Chacón-Patiño, M. L.; Rodgers, R. P. Structure-Reactivity Relationships for Petroleum Asphaltenes. *Energy Fuels* **2022**, *36*, 4370.
(55) Chacón-Patinõ, M. L.; Smith, D. F.; Hendrickson, C. L.; Marshall, A. G.; Rodgers, R. P. Advances in Asphaltene Petroleomics. Part 4. Compositional Trends of Solubility Subfractions Reveal That

https://doi.org/10.1021/acs.energyfuels.2c01541
Energy Fuels 2022, 36, 7542−7557

Polyfunctional Oxygen-Containing Compounds Drive Asphaltene Chemistry. *Energy Fuels* **2020**, *34*, 3013−3030.
(56) Desprez, A.; Bouyssiere, B.; Arnaudguilhem, C.; Krier, G.; Vernex-Loset, L.; Giusti, P. Study of the Size Distribution of Sulfur, Vanadium, and Nickel Compounds in Four Crude Oils and Their Distillation Cuts by Gel Permeation Chromatography Inductively Coupled Plasma High-Resolution Mass Spectrometry. *Energy Fuels* **2014**, *28* (6), 3730−3737.
(57) Garcia-Montoto, V.; Verdier, S.; Maroun, Z.; Egeberg, R.; Tiedje, J. L.; Sandersen, S.; Zeuthen, P.; Bouyssiere, B. Understanding the Removal of V, Ni and S in Crude Oil Atmospheric Residue Hydrodemetallization and Hydrodesulfurization. *Fuel Process. Technol.* **2020**, *201*, 106341.
(58) Snowdon, L. R.; Volkman, J. K.; Zhang, Z.; Tao, G.; Liu, P. The Organic Geochemistry of Asphaltenes and Occluded Biomarkers. *Org. Geochem.* **2016**, *91*, 3−15.
(59) Orea, M.; López, L.; Ranaudo, M. A.; Faraco, A. K. Saturated Biomarkers Adsorbed and Occluded by the Asphaltenes of Some Venezuelan Crude Oils: Limitations in Geochemical Assessment and Interpretations. *J. Pet. Sci. Eng.* **2021**, *206*, 109048.
(60) Acevedo, N.; Moulian, R.; Chacon-Patino, M. L.; Mejia, A.; Radji, S.; Daridon, J.-L.; Mangote, C.; Giusti, P.; Rodgers, R. P.; Piscitelli, V.; Castillo, J.; Carrier, H.; Bouyssiere, B. Understanding Asphaltene Fraction Behavior through Combined Quartz Crystal Resonator Sensor, FT-ICR MS, GPC ICP HR-MS and AFM Characterization. Part I: Extrography Fractionation. *Energy Fuels* **2020**, *34* (11), 13903−13915.
(61) Acevedo, S.; Cordero T, J. M.; Carrier, H.; Bouyssiere, B.; Lobinski, R. Trapping of Paraffin and Other Compounds by Asphaltenes Detected by Laser Desorption Ionization-Time of Flight Mass Spectrometry (LDI-TOF MS): Role of A1 and A2 Asphaltene Fractions in This Trapping. *Energy Fuels* **2009**, *23* (2), 842−848.
(62) Evdokimov, I. N.; Fesan, A. A.; Losev, A. P. Occlusion of Foreign Molecules in Primary Asphaltene Aggregates from Near-UV-Visible Absorption Studies. *Energy Fuels* **2017**, *31* (2), 1370−1375.

https://doi.org/10.1021/acs.energyfuels.2c01541
Energy Fuels 2022, 36, 7542−7557